



HAL
open science

A numerical investigation of heat transfer and pressure drop correlations in Gyroid and Diamond TPMS-based heat exchanger channels

Clement Renon, Xavier Jeanningros

► To cite this version:

Clement Renon, Xavier Jeanningros. A numerical investigation of heat transfer and pressure drop correlations in Gyroid and Diamond TPMS-based heat exchanger channels. *International Journal of Heat and Mass Transfer*, 2025, 239, pp.126599. 10.1016/j.ijheatmasstransfer.2024.126599 . cea-04896410

HAL Id: cea-04896410

<https://cea.hal.science/cea-04896410v1>

Submitted on 19 Jan 2025

HAL is a multi-disciplinary open access archive for the deposit and dissemination of scientific research documents, whether they are published or not. The documents may come from teaching and research institutions in France or abroad, or from public or private research centers.

L'archive ouverte pluridisciplinaire **HAL**, est destinée au dépôt et à la diffusion de documents scientifiques de niveau recherche, publiés ou non, émanant des établissements d'enseignement et de recherche français ou étrangers, des laboratoires publics ou privés.

Title: A numerical investigation of heat transfer and pressure drop correlations in Gyroid and Diamond TPMS-based heat exchanger channels

Authors: Clément RENON^{a,*}, Xavier JEANNINGROS^a

a: CEA, DES, IRESNE, Nuclear Technology Department, Center of Cadarache F-13108 Saint Paul-Lez-Durance, France

*: corresponding author; email address: clement.renon@cea.fr

Keywords

molten salt, heat exchanger, TPMS structure, Nusselt number, friction factor, correlation

Highlights (max 85 characters including spaces)

- Thermohydraulic performance of TPMS channels were investigated numerically
- Correlations were developed for the Nusselt number and the friction factor
- Results are independent of hydraulic diameter and structure density
- A viscosity correction factor was introduced to characterize heat transfers

Abstract

The recent advances in metal additive manufacturing technologies have made TPMS (triple periodic minimal surface) structures a promising alternative for the design of heat exchangers. This numerical study has characterized the thermohydraulic performance of heat exchange channels based on Schwarz-diamond and Schoen-gyroid TPMS structures. The operating ranges applicable to molten salt reactor intermediate exchangers, which have been little studied in the existing literature, were investigated ($2961 < Re < 18254$; $3 < Pr < 5$; $4\text{mm} < d_h < 12\text{mm}$). On the basis of these numerical calculations, two correlations were established to characterize the heat transfer coefficient and the friction factor of such flows. In addition to the classical dependencies observed for Reynolds and Prandtl numbers, an additional parameter was identified to characterize heat exchange, thereby accounting effects of wall boundary conditions. This parameter is defined as the ratio between the mean viscosity of the fluid and its viscosity evaluated at wall temperature. Moreover, the expressions obtained to characterize the Nusselt number and the friction factor are independent of the hydraulic diameter of the channels (serving as a characteristic length) and the density (or porosity) of the TPMS structures. Finally, while both structures exhibit comparable thermal performance, the Schwarz-diamond TPMS appears to be the optimal choice for heat exchanger application, as it involves less pressure drop than Schoen-gyroid TPMS.

Nomenclature

A	area (m ²)
C_p	fluid specific heat capacity (J.kg ⁻¹ .K ⁻¹)
d_h	hydraulic diameter (m)
f	Fanning friction factor (-)
h	convective heat transfer coefficient (W.m ⁻² .K ⁻¹)
L	unit cell size (m)
\dot{m}	mass flow (kg.s ⁻¹)
Nu	Nusselt number (-)
Pr	Prandtl number (-)
Q	heat exchange rate (W)
Re	Reynolds number (-)
T	temperature (K)
t	thickness (m)
v	velocity (m.s ⁻¹)
V	volume (m ³)
y^+	non-dimensional first mesh layer height (-)
z	z-axis
Z	distance along z-axis (m)
Greek symbols	
ΔP	pressure drop (Pa)
ε	TPMS structure porosity (-)
λ	fluid thermal conductivity (W.m ⁻¹ .K ⁻¹)
μ	fluid dynamic viscosity (Pa.s ⁻¹)
ρ	fluid density (kg.m ⁻³)
ϕ	TPMS structure density (-)
Subscripts	
<i>cell</i>	unit cell
<i>cross</i>	cross-sectional
<i>f</i>	fluid
<i>i</i>	inlet
<i>o</i>	outlet
<i>s</i>	solid
<i>s-f</i>	solid-fluid interface
<i>w</i>	wall

1 Introduction

The field of molten-salt reactors (MSRs) has witnessed a resurgence in international activity, with new players focusing on the potential of liquid fuel in nuclear power (reprocessing of spent fuel and long-lived waste). In a loop MSR concept, the thermal performance of heat exchangers is one of the technical design challenges.

Until now, the majority of heat exchangers used in industry have been based on a succession of tubes or plates, whose morphology can be modified to favor heat transfers [1,2]. However, recent technological advances in metal additive manufacturing have made it possible to create new three-dimensional exchange patterns. The structures under consideration typically exhibit periodic patterns with a high exchange surface-to-volume ratio. Among them, the Triple Periodic Minimal Surfaces (TPMS) have recently emerged as a subject of particular interest [3,4]. This family of mathematical surfaces, most often defined on the basis of parametric equations, allows the creation of two independent, intertwined three-dimensional channels, which form the basis of heat exchanger design [5]. In recent years, several studies have indicated that these structures offer superior performance to conventional heat exchanger technologies, including tubes and shells, plates, and so forth [3,4].

Among the various TPMS geometries, the Schwarz-primitive (P), Schoen-gyroid (G) and Schwarz-diamond (D) structures have been the subject of the most extensive research in the literature. G and D structures are of particular interest, while many studies agree that P structures offers less performance gain, because of limited mixing of streamlines [6,7] which are unable to generate sufficient fluid disturbance to enhance heat transfer [8]. The good thermal performance of G and D structures is due to the highly 3D flows. Given the inherent difficulty of conducting experimental observations of these flows, only numerical studies have been carried out. These include the work of Liang et al. [9] and Li et al. [10], which highlight the helical flow in this type of structure, involving strong fluid stirring and interactions between the different channels (in contrast to the low-velocity backflow regions observed in P structures). In particular, structure D exhibits both clockwise and counter-clockwise helical motion of streamlines in the flow direction, which implies the presence of shear zones at each flow crossing. The study by Yan et al. [8] emphasizes the significance of these circulation and shear zones, even at low flow Reynolds numbers ($Re < 500$) with water.

Other TPMS structures have also been studied by some authors, such as Fisher Koch S [7,11,12], F-RD [7,12], I-WP [8,11,12] and Neovius [7,12]. In particular, hybrid TPMS structures have been proposed by Xu et al. [13] but the gain in the ratio of heat exchange and pressure drop has not been observed. The present study will focus on Schoen-gyroid (G) and Schwarz-diamond (D) TPMS structures.

The majority of studies dealing with the thermohydraulic performance of TPMS G and D patterns are numerical CFD RANS studies. In most studies, the flows under investigation are typically water or air, operating at low Reynolds numbers (below 1000). Peng et al. [14] studied the gyroid pattern with a conjugated heat transfer calculation, fixing the wall thickness at 1mm (based on manufacturing tests, which demonstrated that walls thickness less than 0.2mm were not achievable). Alteneiji et al [6] studied a gyroid crossflow heat exchanger, as Yan et al. [8] did for gyroid and diamond patterns, for turbulent flow, but at relatively low Reynolds number ($Re < 500$). A similar study was also carried out by Li et al. [15] in the context of supercritical CO₂ exchangers, at higher Reynolds numbers (up to $Re = 70000$). Iyer et al. [7] also carried out a series of numerical calculations, for water flows at low Reynolds numbers ($Re < 300$), for various TPMS geometries, and proposed several correlations linking the Nusselt number and the friction factor to the Reynolds number. Dixit et al. [16] carried out a numerical/experimental comparison in the context of a cross-flow gyroid exchanger, but for very low

Reynolds flows (10-40). Liang et al. [17] exploited a polymer heat exchanger in cross-flow configuration, for air flow, testing various TPMS geometries and different hydraulic diameters and porosities. All these studies agree that G and D patterns offer a performance advantage over conventional channel geometries.

Finally, in the recent experimental and numerical study by Yan et al. [18] the authors sought to characterize heat exchange and pressure drop in a TPMS gyroid-based cross-flow exchanger, for turbulent water flow ($150 < Re < 3000$). The authors propose two correlations linking the Nusselt number to the Prandtl and Reynolds numbers, and the friction factor to the Reynolds number. A slight increase in the Nusselt number is observed experimentally compared with the numerical calculations. A discrepancy was also observed between the experimental and numerical pressure drop measurements, with a range of values from 9.7% to 69.8%. The authors attribute these effects to the wall roughness inherent in the manufacturing process (the channels studied have a relatively small hydraulic diameter, with a value of $d_h = 1.56\text{mm}$).

However, all the studies cited above characterize and compare exchange patterns by considering the length of the elementary cell and the wall thickness of the pattern. As a result, these results are highly dependent on geometric choices. Reynolds et al. [12], in their experimental study, took the approach of considering only the hydraulic diameter as the characteristic length, and porosity as the second parameter: the unit cell length and wall thickness derived from these two parameters. They propose a correlation for convective exchanges for the gyroid pattern depending only on Reynolds and Prandtl numbers, without observing any influence of geometric parameters.

The objective of this numerical study is to identify the key parameters governing heat transfer and pressure drop in gyroid and diamond-based TPMS exchange matrices, in order to provide all the elements needed to design heat exchangers, regardless of the geometric parameters considered (elementary cell size, wall thickness, etc.). To this end, correlations for estimating heat exchange and pressure drop have been developed. In particular, this study will focus on exploring the operating ranges applicable to molten-salt reactor intermediate exchangers, little studied in the literature ($2961 < Re < 18254$; $3 < Pr < 5$; $4\text{mm} < d_h < 12\text{mm}$; high heat flux density $\sim 1\text{ MW/m}^2$).

2 Problem modeling

2.1) TPMS Structures

This study deals with Schoen-gyroid (G) and Schwarz-diamond (D) TPMS, which can be approximated by the following equations, where x , y and z are Cartesian coordinates.

TPMS Schoen-gyroid:

$$\psi(x, y, z) = \sin(x) \cos(y) + \sin(y) \cos(z) + \sin(z) \cos(x) = C \quad (1)$$

TPMS Schwarz-diamond:

$$\psi(x, y, z) = \sin(x) \sin(y) \sin(z) + \sin(x) \cos(y) \cos(z) + \cos(x) \sin(y) \cos(z) + \cos(x) \cos(y) \sin(z) = C \quad (2)$$

$\psi(x, y, z)$ is an isosurface evaluated at iso value C .

It is then possible to define a volume such that $\psi(x, y, z) > C$ or $\psi(x, y, z) < C$ (solid lattice), or create a solid thickness defined by $-C < \psi(x, y, z) < C$ (sheet lattice).

By generating a solid thickness t_s with this second approach, it is possible to obtain elementary cubic exchange patterns of side L , as shown in Fig. 1. These types of patterns split the volume into two independent circuits of equal volumes, making it possible to circulate two fluids in counter-flow and create a heat exchanger, as illustrated in Fig. 2. The exchange matrix is formed by the repetition of an elementary cubic pattern, whose geometry depends on the choice of solid wall thickness t_s and unit cell length L (edge of the elementary cube).

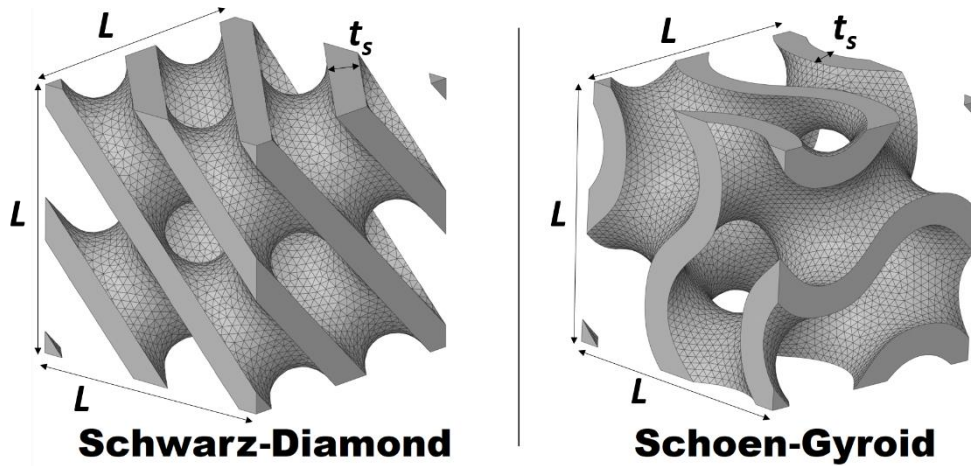


Fig. 1: Two examples of Schwarz-diamond (D) and Schoen-gyroid (G) unit cells (solid domain)

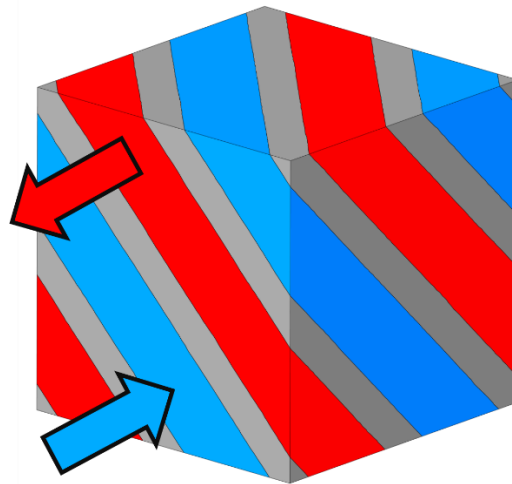


Fig. 2: Representation of both fluids volumes (blue and red) and solid volumes (grey) of a Schwarz-diamond unit cell. Arrows indicate a counter-flow exchanger configuration.

For the purposes of this study, the geometries were generated using the Open Source software MSLattice [19]. Subsequently, these geometries were subjected to further modifications in order to be able to use them for CFD calculations with ANSYS Fluent software. This process entails the regularization of the facetized body and the rectification of potential geometric imperfections that could interfere with the generation of the mesh or the implementation of boundary conditions.

However, while knowledge of t_s and L alone can characterize the geometry under study, they are not very well suited to characterizing flows and obtaining generic correlations.

It is therefore necessary to determine a reference length characterizing the fluid channel, particularly in order to define the Reynolds number. While some authors use the pore size, the hydraulic diameter

seems to be the most suitable for characterizing channel size [3,20]. The hydraulic diameter is defined here in a similar manner to numerous articles [4,7,8,11,12] dealing with TPMS, using the following equation:

$$d_h = \frac{4 V_f}{A_{s-f}} \quad (3)$$

Where V_f is the fluid volume and A_{s-f} the area of the solid-fluid interface.

Moreover, rather than wall thickness, we recommend, like Reynolds et al. [12], characterizing the pattern by its density ϕ (NB: or porosity $\varepsilon = 1 - \phi$), as defined by the following equation:

$$\phi = \frac{V_s}{L^3} \quad (4)$$

Where V_s denotes the solid volume of a cubic unit cell and L the length of the edge.

It turns out, moreover, that these three quantities (t_s , d_h and ϕ) can be linked by the following relationship (demonstration in Appendix A):

$$\phi \simeq \frac{1}{1 + \frac{d_h}{2 t_s}} \quad (5)$$

Simply knowing ϕ and d_h can therefore fully characterize the geometry, since unit cell size L and wall thickness t_s are imposed by the choice of these two parameters. Tab. 1 summarizes the different geometric configurations considered in this study. It should be noted that these quantities were calculated for each respective final geometry using the measurements of A_{s-f} , V_f , and L obtained from the ANSYS Fluent CAD software.

	Schwarz-diamond	Schoen-gyroid
ϕ	0.1362 to 1/3	1/3
d_h (mm)	4 to 12	4 to 8
L (mm)	10.92 to 32.76	8.82 to 17.64
t_s (mm)	0.473 to 3	1 to 2

Tab. 1: Ranges of geometrical parameters considered in this study (min to max values)

2.2) Numerical modeling

The various CFD calculations were performed with ANSYS Fluent 2022R2 software, using RANS k- ω SST turbulence modeling, without wall functions. This modeling decision was, in particular, backed up by the work of Yan et al. [8], who compared different turbulence models ($200 < Re < 4000$). Furthermore, this choice of turbulence modelling corresponds with all the numerical studies referenced in the introduction section dealing with turbulent flows in TPMS channels. The velocity and pressure equations were coupled using the SIMPLE algorithm.

The working fluid is a NaCl-MgCl₂-PuCl₃ [21-23] ternary molten salt, with a mean temperature range of 510°C to 710°C. It should be noted that the thermal properties of such a liquid are relatively close to those of water (the Prandtl number range considered here being between $Pr=3$ and $Pr=5$), which should allow comparison and direct application with other industrial applications.

The aim of this study is to provide data on the thermohydraulic properties of TPMS G and D patterns. To achieve this, the study will seek to determine the general properties of a unit cell representative of the heat exchange pattern core, i.e. in fully developed flow and therefore excluding any possible edge effects. With this in mind, 7 elementary cells are considered, end-to-end along a z axis, as illustrated in Fig. 3. Periodicity conditions are imposed on the 4 side planes of the domain. A mass flow rate and temperature are imposed at the domain inlet. A pressure condition is imposed at the domain outlet. Finally, a uniform wall temperature is imposed at the solid-fluid interface, in order to provide a more straightforward basis for the exploitation and interpretation of the results.

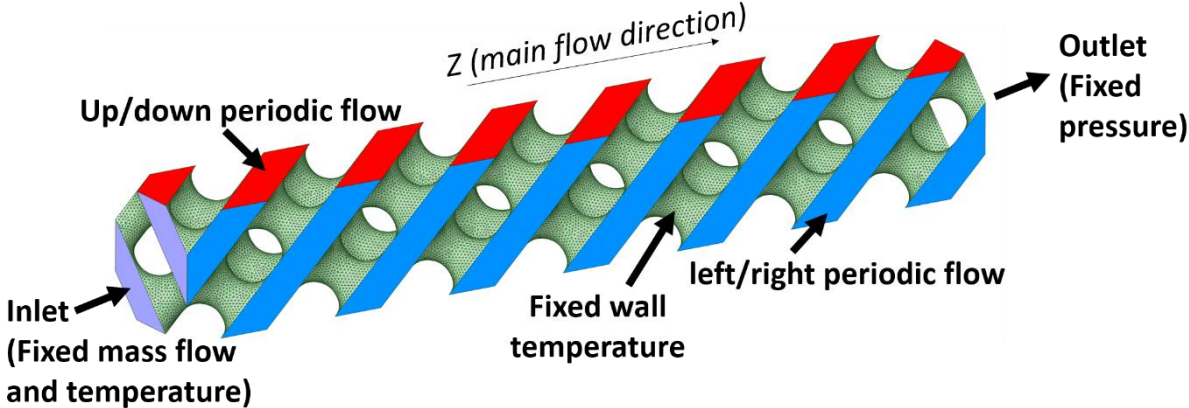


Fig. 3: Representation of boundary conditions around the fluid domain (7 TPMS D unit cells)

The total length of the domain, set at 7 cells, is sufficient for the flow to reach a fully developed state, where the quantities of interest (Nusselt number and fanning friction factor) are stable, as illustrated in Figure 4. Preliminary calculations, carried out under various flow conditions, with longer fluid domains up to 10 elementary cells, showed that it was not necessary to perform calculations over a longer domain. The Nusselt number and the Fanning friction factor reach a plateau value after $Z > 2L$ in all configurations calculated with pattern D: the results are analogous to those observed in Figure 4, exhibiting a reduction in the Nusselt number and fanning friction factor in the two first elementary cells of the fluid domain. This finding is observed for the different flowrate and geometry conditions carried out during this study, and also for pattern G. These observations are also consistent with the work of Samson et al. [20]. Furthermore, due to highly 3D circulations, pressure and temperature fluctuations due to reverse flow at the outlet are frequently observed, as also noted by some authors [7-9]. Consequently, in the following calculations, only the domain located between $2L < Z < 6L$ (i.e. the four cells shown in blue in the illustration in Fig. 4, numbered 3 to 6) will be considered for data processing in order to give representative average conditions, which can provide usable data for designing heat exchangers.

During the calculation process, the key physical data, namely the average pressure and temperature at the inlet and outlet of each elementary cell, are monitored to ensure the requisite convergence of the calculation.

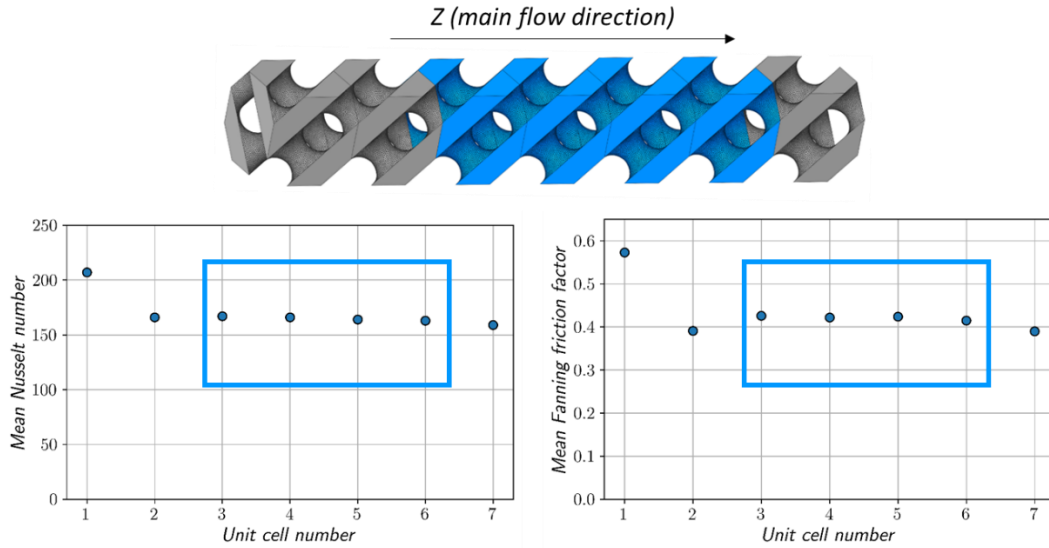


Fig. 4: Longitudinal evolution of the mean Nusselt number and friction coefficient (TPMS D, $d_h=8\text{mm}$, $\Phi=1/3$, $\dot{m}=0.264\text{ kg}\cdot\text{s}^{-1}$). Highlighted blue section refers to the volume of interest.

The domain mesh is refined near the wall, with 15 inflation prism layers with a growth ratio of 1.15 to characterize the boundary layer, and the rest of the domain is composed of unstructured tetrahedral meshes. The size of the first prism layer is chosen to respect $y^+ < 1$. A mesh convergence study was carried out on each geometry to select a mesh density suited to the problem. Both the mean Nusselt number and Fanning friction factor were chosen to determine the mesh independence. Tab. 2 provides a summary of the results for a TPMS D geometry with $d_h=8\text{ mm}$. In this example, the fourth mesh size was selected. For the cases presented in this article, the total number of elements ranges from 10.9 to 23.3 million, depending on the geometry considered.

	Number of mesh (million)	mesh size (μm)	Number of prism layers	First prism height (μm)	Mean Nusselt number	Mean Fanning friction factor
Mesh 1	3.6	500	12	15	171	0.45
Mesh 2	7.1	350	16	5	166	0.43
Mesh 3	9.2	250	10	10	165	0.43
Mesh 4	10.9	250	16	5	165	0.42
Mesh 5	26.0	175	15	2.5	165	0.41

Tab. 2: Evolution of Nusselt number and friction factor for 5 different meshing parameters for a fixed geometry (TPMS D, $d_h=8\text{mm}$, $\Phi=1/3$, $\dot{m}=0.264\text{ kg}\cdot\text{s}^{-1}$).

2.3) Data reduction

As discussed in section [2.1]), the hydraulic diameter, needed to define the Reynolds number, is selected as the characteristic length.

v_z is the mean fluid velocity in the main flow direction, which can be related to the mass flow rate \dot{m} imposed at the domain inlet by the relation :

$$v_z = \frac{\dot{m}}{\rho A_{\text{cross}}} \quad (6)$$

A_{cross} designates the area of the average fluid cross-section (plane orthogonal to the main flow direction), defined as following:

$$A_{cross} = \frac{V_f}{L} \quad (7)$$

It is crucial to highlight that in TPMS-type structures, the cross-sectional area of flow is not uniform along the z-axis. Therefore, it is essential to define the mean cross-sectional area of flow, rather than the cross-sectional area of flow at the domain inlet, which is contingent upon an arbitrary choice of the unit cell periodicity plane [18].

Based on these parameters and the fluid properties, it is possible to define the mean Reynolds number of the flow (in the fluid volume of interest located for $2L < Z < 6L$):

$$Re = \frac{\rho v_z d_h}{\mu} \quad (8)$$

With ρ the density and μ the dynamic viscosity of the fluid. These fluid properties are evaluated at temperature T_{mean} defined as the mean temperature of the fluid domain for $2L < Z < 6L$.

The Prandtl number of the liquid is defined according to the following equation, each property taken at temperature T_{mean} :

$$Pr = \frac{\mu Cp}{\lambda} \quad (9)$$

Where λ is the thermal conductivity of the fluid, taken constant at $0.5 \text{ W.m}^{-1}.\text{K}^{-1}$ and Cp is the specific heat capacity of the fluid.

In order to characterize heat exchange at the wall, the local heat transfer coefficient h_{cell} is defined as follows, where Q_{cell} is the heat exchange rate at the solid-fluid interface of area A_{s-f} , T_w is the local wall temperature and T_{mean} is the reference temperature:

$$h_{cell} = \frac{Q_{cell}}{(T_w - T_{mean}) A_{s-f}} \quad (10)$$

Since a constant wall temperature is imposed by the model (see section [2.2]), determining h_{cell} means determining the heat transfer rate Q_{cell} when the fluid passes through a unit cell. This value is calculated by performing an energy balance at the unit cell level:

$$Q_{cell} = \dot{m} Cp (T_o - T_i) \quad (11)$$

Where T_i is the mean temperature of the flow cross-section at the unit cell inlet and T_o is at the unit cell outlet.

In the subsequent analysis, the non-dimensional Nusselt number will be employed:

$$Nu_{cell} = \frac{h_{cell} d_h}{\lambda} \quad (12)$$

The mean Nusselt number value (Nu) obtained over the 4 cells of interest in the study domain ($2L < Z < 6L$) will then be considered.

Furthermore, for heat exchanger design, knowledge of pressure drops is required. A Fanning friction factor f_{cell} evaluated on a unit cell is defined according to the following equation:

$$f_{cell} = \frac{\Delta P_{cell} d_h}{2 L \rho v_z^2} \quad (13)$$

Where ΔP_{cell} corresponds to the pressure drop between the inlet and outlet of an elementary cell.

Hereafter, the mean f value obtained for the 4 cells of interest in the domain ($2L < Z < 6L$) will be considered.

3 Results and discussion

3.1) Heat exchange

Fig. 5 illustrates the mean Nusselt number variation as a function of the Reynolds number for a fixed geometry (TPMS D, $\Phi=1/3$, $d_h=8\text{mm}$) and a fixed Prandtl number ($Pr=4.06\pm 1.7\%$) (N.B.: due to the increase in mixture temperature, a slight discrepancy in average fluid properties is observed between the different cases plotted on the graph). In these different configurations, the wall temperature is set at 793K and the inlet temperature at 883K: the fluid cools the wall. In line with what is classically observed in the literature, the average Nusselt number increases with the Reynolds number. It should be noted that all the configurations studied in this study correspond to a turbulent flow regime. The Reynolds numbers considered are between $Re=2961$ and $Re=18254$. The turbulent transition for this type of pattern is observed for much lower Reynolds numbers, in the range of $Re = 150 \sim 300$, according to Dybbs et al. [24].

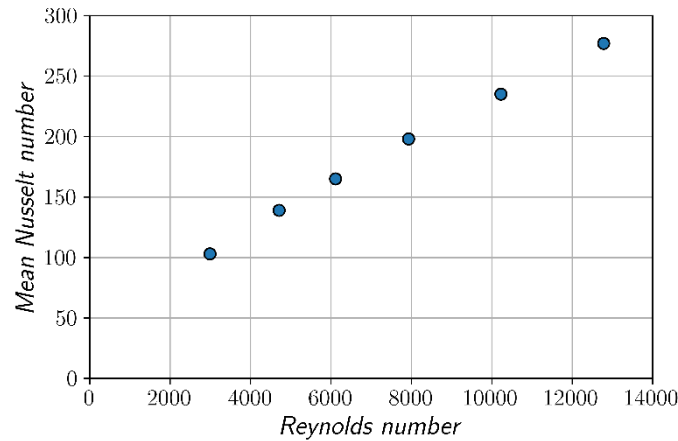


Fig. 5: Mean Nusselt number versus Reynolds number (TPMS D, $d_h = 8\text{mm}$, $\Phi=1/3$, $Pr=4.06\pm 1.7\%$, $\mu/\mu_w = 0.83\pm 1.7\%$)

By varying the inlet temperature and the wall temperature, it is also possible to vary the mean Prandtl number of the fluid. Fig. 6 illustrates the variation of the mean Nusselt number as a function of the Prandtl number, for the same geometry and fixed Reynolds number ($Re=6010\pm 1.4\%$). As is conventionally observed in the literature, an increase in the Prandtl number induces an increase in the mean Nusselt number due to the thinning of the thermal boundary layer. It should also be noted that a $Pr^{1/3}$ trend, widely used in the literature to describe convective transfers, provides good agreement

with the present data, even with geometry as tortuous as TPMS-based channels. This exponent is also the one used in the correlations established by Cheng et al. [25] and Yan et al. [18] for TPMS structures, but is different from Reynolds et al.'s proposal for air [12] ($Pr^{0.4}$).

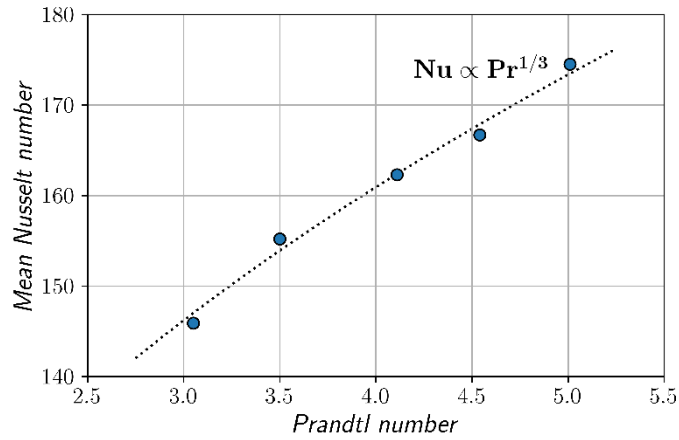


Fig. 6: Mean Nusselt number versus Prandtl number: points from CFD calculations versus theoretical $Pr^{1/3}$ dependence (TPMS D, $d_h=8\text{mm}$, $\Phi=1/3$, $Re=6010\pm 1.4\%$, $\mu/\mu_w=0.805\pm 1.6\%$)

These dependencies on Prandtl and Reynolds numbers have already been the subject of some studies, as mentioned in the introduction. However, in a nuclear reactor intermediate heat exchanger application, the heat fluxes and temperature differences involved can be significant, so that the wall temperature boundary condition can also be shown to have an influence on the average Nusselt number. This is particularly true when comparing a configuration where the fluid is heated by the wall, or on the contrary, cooled by the wall. Fig. 7 presents a comparison of the evolution of the mean Nusselt number for the same geometry at different Reynolds numbers, with the fluid being cooled ($T_i=883\text{K}$, $T_w=793\text{K}$) and heated ($T_i=793\text{K}$, $T_w=883\text{K}$). The Nusselt number is here divided by $Pr^{1/3}$ to avoid the influence of Prandtl number variation.

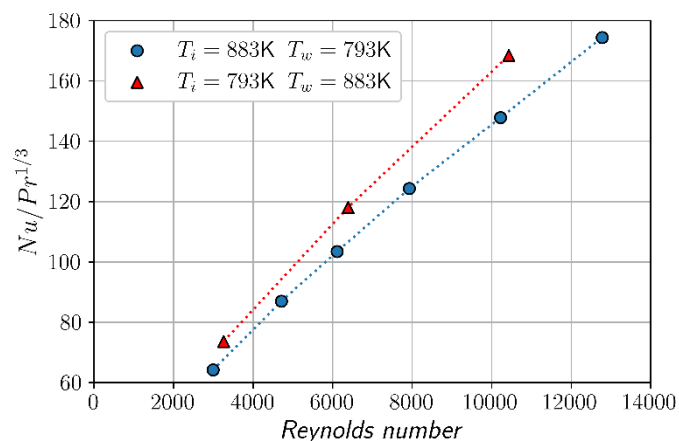


Fig. 7: $Nu/Pr^{1/3}$ versus Reynolds number for two different temperature conditions (TPMS D, $d_h=8\text{mm}$, $\Phi=1/3$)

The difference observed between these two curves is attributed to the variation in the properties of the near-wall fluid, especially its viscosity, as generally suggested in other applications where this

phenomenon is impactful [26]. The use of the corrective ratio, μ/μ_w , initially introduced by Sieder and Tate [27] for tubular flows, is therefore recommended in order to fully characterize the mean Nusselt number. This is the ratio of the mean fluid viscosity μ evaluated at T_{mean} temperature to the fluid viscosity evaluated at wall temperature μ_w . This influence, although of second order compared to the influence of Re and Pr , is important to take into account when designing heat exchangers, where the Nusselt number must be estimated on both sides of the exchanger (either in "heated" fluid configuration ($\mu/\mu_w < 1$) or "cooled" fluid configuration ($\mu/\mu_w > 1$)). Tab. 3 shows results obtained for a substantially identical mean Reynolds and Prandtl numbers, with the same molten salt, but with different temperature configurations (configurations denoted A and B). An increase of 10.3% in the Nusselt number value is observed when moving from a wall temperature of 755K to 883K, underlining the importance of considering this third parameter in certain applications. A third C configuration was calculated for a molten salt of different composition. An analogy with Reynolds and Prandtl numbers and μ/μ_w ratio with configuration B shows that the calculated Nusselt number is substantially identical, although the temperatures and heat fluxes involved are different. This calculation, along with other configurations tested, confirms that Re , Pr and μ/μ_w can be used to characterize heat exchange for a flow that corresponds to the ranges under investigation in this study.

Configuration	Salt	Reynolds number	Prandtl number	μ/μ_w	T_{mean}	T_w	Flux density (absolute value)	Nusselt number
A	NaCl-MgCl ₂ - PuCl ₃	6348	4.45	0.81	826 K	755 K	775 kW/m ²	173.6
B	NaCl-MgCl ₂ - PuCl ₃	6384	4.46	1.35	825 K	940 K	1375 kW/m ²	191.4
C	NaCl-MgCl ₂	6387	4.44	1.35	817 K	883 K	799 kW/m ²	193.6

Tab. 3: Effect of μ/μ_w on Nusselt number in iso- Re and iso- Pr configurations.

The preceding discussions concern a fixed geometry. Fig. 8 shows the $(Nu/Pr^{1/3})$ value calculated for various TPMS D structure densities ($0.1362 < \Phi < 1/3$) and hydraulic diameters ($4\text{mm} < d_h < 12\text{mm}$). The μ/μ_w ratio was set at $0.83 \pm 2.1\%$ for all configurations. These calculations show that no significant variation appears when the same Reynolds number is considered. These results are consistent with the experimental observations of Reynolds et al. [12] with air and confirm the relevance of parameterizing the geometry using d_h and Φ for the purpose of comparing disparate geometries, rather than t_s and L , which is a common practice in the literature (see introduction [1]).

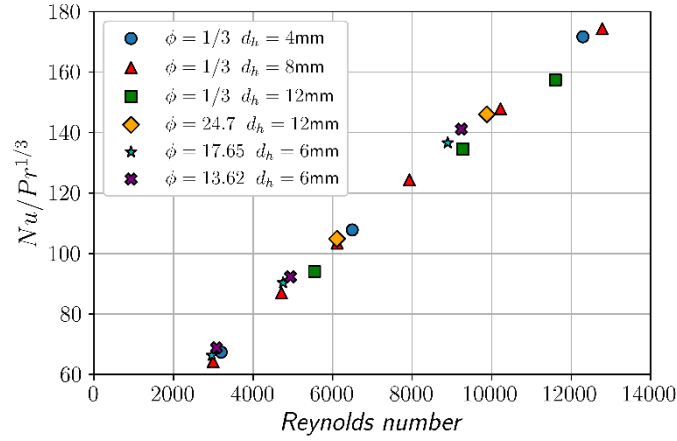


Fig. 8: $Nu/Pr^{1/3}$ versus Reynolds number for various hydraulic diameter and density values (TPMS D, $\mu/\mu_w = 0.83 \pm 2.1\%$).

Fig. 9 compares TPMS G and D geometries. No significant difference in heat exchange is observed for the range of parameters investigated in this study. This suggests that the comments made above also apply to TPMS G.

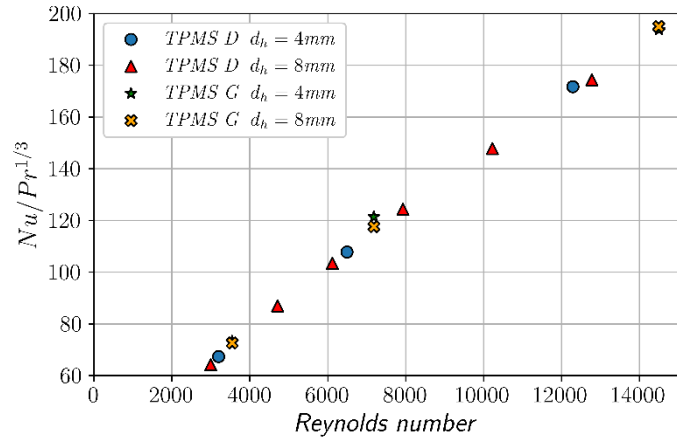


Fig. 9: $Nu/Pr^{1/3}$ versus Reynolds number. Comparison between TPMS D and G geometries ($\mu/\mu_w = 0.83 \pm 2.1\%$, $\Phi = 1/3$)

Considering 40 configurations studied with the TPMS D pattern, for different flow conditions ($2961 < Re < 18254$; $3 < Pr < 5$), wall boundary conditions ($0.79 < \mu/\mu_w < 1.39$), and geometries (d_h ; Φ ; Tab. 1), it was possible to determine a correlation using a least squares method. In line with the observations described above, a relationship of the form $Nu = f(Re, Pr^{1/3}, \mu/\mu_w)$ was sought. The following equation is obtained:

$$Nu = 0.2644 Re^{0.69} Pr^{1/3} \left(\frac{\mu}{\mu_w}\right)^{0.20} \quad (14)$$

This equation fits the CFD data very satisfactorily, with an average relative error of 1.60% and a maximum relative error of 5.48% over all the configurations studied (see Fig. 10). This equation accounts for the mean Nusselt number obtained over an entire TPMS D unit cell, for a fully developed flow, and uniform wall temperature. In accordance with the observations shown in the Fig. 9, this equation also appears to be applicable to a lesser extent to TPMS G geometries. This equation applies to the conditions and parameter ranges mentioned above.

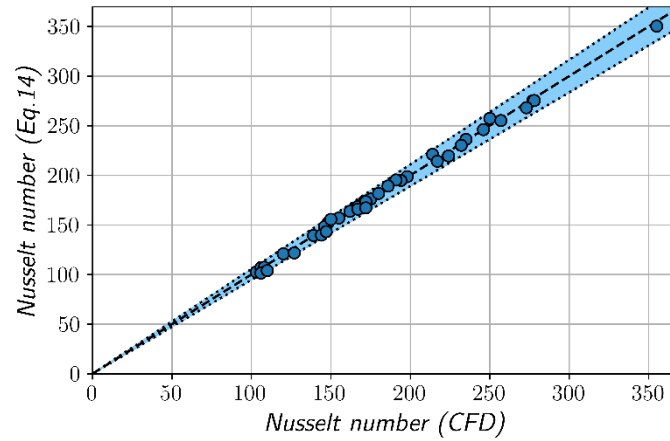


Fig. 10: Mean Nusselt number from Eq. 15 versus the calculated values. Dotted lines refer to the max relative error ($\pm 5.48\%$)

Comparing this correlation with those in the literature [7,12,18] is difficult, because these equations are established for different data ranges (see Tab. 4). However, it is possible to a lesser extent to compare the Eq. 14 to the equation established by Yan et al. [18], as illustrated in Fig. 11 (NB: a fixed $\mu/\mu_w=1$ ratio is considered for the comparison, since this parameter is not taken into account in the study by Yan et al. [18], and the data for establishing their correlation are fairly distributed in “heated fluid” and “cooled fluid” configurations). Despite the methodological differences between these two studies, the numerical results presented here fit very well with the experimental data of Yan et al. [18], even when extrapolating correlations for a wider Reynolds number range. In their correlation, the exponent associated with the Reynolds number ($Re^{0.627}$) is slightly lower than in the correlation developed here ($Re^{0.69}$), which could be attributed to the higher Reynolds numbers investigated in this study compared to that of Yan et al. [18]. This is consistent with the experimental correlation developed by Reynolds et al. [12]. The correlations proposed by Iyer et al. [7], for laminar or transient flow regimes at low Reynolds numbers, have a much lower exponent ($Re^{0.55-0.57}$) than the other studies.

Authors	Type of data	TPMS structure	Range of Re	Range of Pr	Nu correlation
Iyer et al. [7]	numerical	D	15 - 300	6.97	$Nu = 2.24 Re^{0.55}$
Iyer et al. [7]	numerical	G	20 - 250	6.97	$Nu = 1.48 Re^{0.57}$
Reynolds et al. [12]	experimental	G	100 - 2500	0.7	$Nu = 0.49 Re^{0.62} Pr^{0.4}$
K.Yan et al. [18]	experimental	G	150 - 3000	3.5 - 9	$Nu = 0.471 Re^{0.627} Pr^{1/3}$

Tab. 4: Summary of TPMS D and G mean Nusselt number correlations

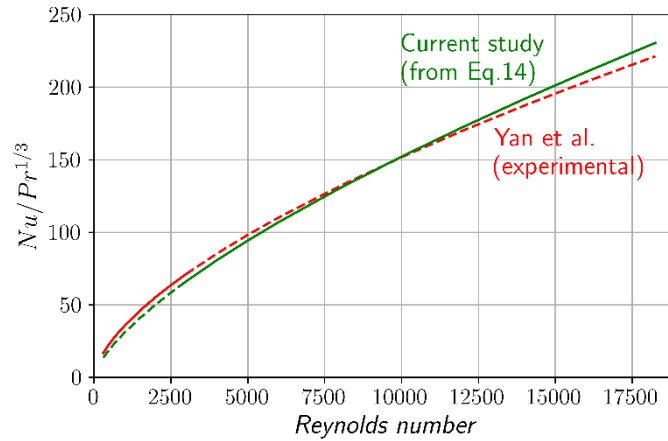


Fig. 11: Comparison between Eq. 16 and Yan et al. [18] experimental correlation, with $\mu/\mu_w = 1$. Dotted lines refers to out-of-range Reynolds numbers for respective studies.

The correlation proposed in this study therefore makes it possible to estimate the Nusselt number for a wide range of Reynolds and Prandtl numbers, while maintaining consistency with the abovementioned experimental measurements. The Eq. 14 can also be employed to incorporate an additional parameter, the μ/μ_w corrective ratio, which may be of significance in certain industrial applications where the heat fluxes are high and the liquid properties variable.

3.2) Pressure drops

Knowing the pressure drop across the exchange pattern is a key element in interpreting the performance of a heat exchanger.

The graph in Fig. 12 illustrates the effect of varying the Reynolds number on the friction factor in a TPMS D geometry, for various Prandtl number, μ/μ_w ratio, hydraulic diameter d_h , and density Φ (40 calculations). The Reynolds number value alone provides a good estimate of the friction factor in this type of pattern. The other parameters mentioned above have no clearly identifiable effect, as also noted by [7,12,18].

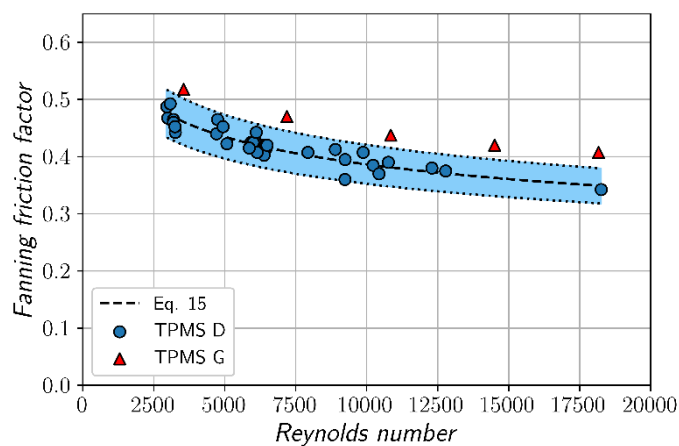


Fig. 12: Mean Fanning friction factor versus Reynolds number: Eq. 17 and CFD points. Dotted lines refers to the maximum relative error ($\pm 8.82\%$)

The graph in Fig. 12 also illustrates the effect of a variation of the Reynolds number on the friction factor for some configurations calculated with a TPMS G geometry. It can be observed that, for an identical Reynolds number, the friction factor is greater for the G structure than for the D. An increase

of 12.3% to 16.7% for coefficient f on the configurations studied is observed. A similar phenomenon was also observed by [12] in low Reynolds configurations under laminar flow conditions.

Since heat exchange is similar for the two types of geometries (see results presented in paragraph [3.1]), a heat exchange matrix based on the TPMS D geometry performs better than TPMS G at a fixed Reynolds number for the range of parameters studied here. TPMS D therefore seems preferable for heat exchanger design.

The graph in Fig. 13 compares the friction factors obtained for the G structure with the experimental and numerical data of Reynolds et al. [12] and Yan et al. [18]. To enable direct comparison, three additional points outside the present study range, at lower Reynolds, have been calculated and plotted. There is good agreement with the variations observed experimentally by Reynolds et al. [12] with air and numerically by Yan et al. [18] with water. However, the latter's experimental data give a much higher friction factor, which the authors attribute to the wall roughness present in the model studied (the hydraulic diameters of the channels under consideration have a relatively small value of d_h , with a value of 1.56mm).

From the 40 configurations calculated for the TPMS D geometry, it is also possible to extract a correlation using a least-squares method:

$$f = 1.850 Re^{-0.17} \quad (18)$$

This equation correlates the CFD data with an average relative error of 2.42% and a maximum error of 8.82% (see Fig. 12). This equation accounts for the mean friction factor of a TPMS D elementary cell in a fully developed flow. This equation is applicable to the same range of parameters as the correlation [Eq. 14], thus encompassing a broader Reynolds range than that observed in the aforementioned experimental studies.

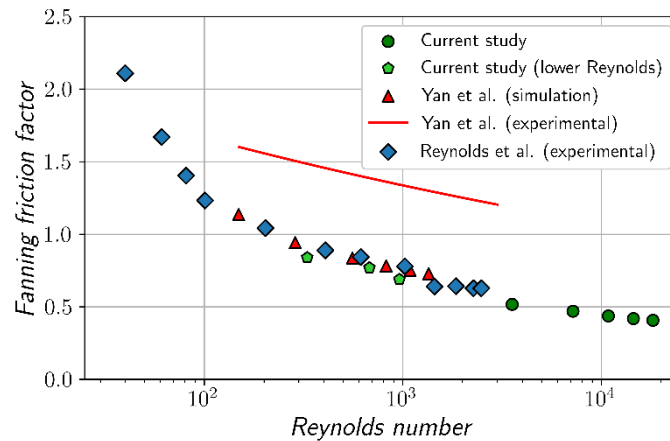


Fig. 13: Comparison between Fanning friction factor from current study versus Yan et al. [18] and Reynolds et al. [12] studies, for TPMS gyroid structures.

4 Conclusion

A numerical study has been carried out to characterize the thermohydraulic performance of heat exchange channels based on Schwarz-diamond and Schoen-gyroid TPMS structures. On the basis of numerical calculations, a correlation relating the Nusselt number to the Reynolds number, the Prandtl number, and the μ/μ_w ratio was proposed, as well as a correlation relating the friction factor to the

Reynolds number. These correlations will prove useful for sizing heat exchangers based on Schwarz-diamond TPMS, particularly for nuclear applications, whose parameter ranges have hitherto been poorly represented in the literature.

Several highlights emerge from this study:

- (1) The thermal performance of Schoen-gyroid and Schwarz-diamond TPMS structures is identical for the range of parameters investigated in this study. Consequently, the Nusselt number correlation is applicable to both structures.
- (2) Nevertheless, Schoen-gyroid TPMS have higher pressure drops, with the same set of parameters, than Schwarz-diamond TPMS structures, which seem preferable for the design of heat exchangers.
- (3) The expressions obtained to characterize the Nusselt number and the friction factor are independent of the density ϕ and the hydraulic diameter: no dependence was observed, which underlines the interest of choosing these two parameters to characterize TPMS geometries.
- (4) An additional parameter was considered for characterizing heat exchange with regard to the literature on TPMS study: the μ/μ_w corrective ratio. This parameter can be used to take into account the influence of wall heating of the fluid, and is particularly suitable for the conditions encountered in intermediate heat exchangers for molten salt reactors.

Further work

An experimental metal model, manufactured by powder bed fusion 3D printing, is currently being designed to experimentally confirm these numerical calculations for the same range of parameters (Reynolds and Prandtl equivalence). A particular focus will be put on investigating the potential effects of wall roughness.

Appendix A

In the situation where the two fluid volumes V_f are identical, the latter can be related to the geometric parameters of the unit cell according to the following equation:

$$V_f = \frac{(1 - \phi) L^3}{2} \quad (16)$$

When t_s is small compared to d_h , which is generally the case in heat exchanger applications, the following equation provides a good estimate of the solid-fluid interface area A_{s-f} :

$$A_{s-f} \simeq \frac{V_s}{t_s} = \frac{\phi L^3}{t_s} \quad (17)$$

Eq. 3 can then be reformulated using Eqs. 16 and 17:

$$d_h \simeq \frac{2(1 - \phi) t_s}{\phi} \quad (18)$$

Isolating ϕ in the Eq. 18 yields the Eq. 5.

References

- [1] T.M. Abou Elmaaty, A.E. Kabeel, M. Mahgoub, Corrugated plate heat exchanger review, *Renew. Sustain. Energy Rev.* 70 (2017) 852–860. <https://doi.org/10.1016/j.rser.2016.11.266>.
- [2] S.A. Marzouk, M.M. Abou Al-Sood, E.M.S. El-Said, M.M. Younes, M.K. El-Fakharany, A comprehensive review of methods of heat transfer enhancement in shell and tube heat exchangers, *J. Therm. Anal. Calorim.* 148 (2023) 7539–7578. <https://doi.org/10.1007/s10973-023-12265-3>.
- [3] K. Yeranee, Y. Rao, A Review of Recent Investigations on Flow and Heat Transfer Enhancement in Cooling Channels Embedded with Triply Periodic Minimal Surfaces (TPMS), *Energies* 15 (2022). <https://doi.org/10.3390/en15238994>.
- [4] K. Dutkowski, M. Kruzel, K. Rokosz, Review of the State-of-the-Art Uses of Minimal Surfaces in Heat Transfer, *Energies* 15 (2022). <https://doi.org/10.3390/en15217994>.
- [5] T. Femmer, A.J.C. Kuehne, M. Wessling, Estimation of the structure dependent performance of 3-D rapid prototyped membranes, *Chem. Eng. J.* 273 (2015) 438–445. <https://doi.org/10.1016/j.cej.2015.03.029>.
- [6] M. Alteneiji, M.I.H. Ali, K.A. Khan, R.K.A. Al-Rub, Heat transfer effectiveness characteristics maps for additively manufactured TPMS compact heat exchangers, *Energy Storage Sav.* 1 (2022) 153–161. <https://doi.org/10.1016/j.enss.2022.04.005>.
- [7] J. Iyer, T. Moore, D. Nguyen, P. Roy, J. Stolaroff, Heat transfer and pressure drop characteristics of heat exchangers based on triply periodic minimal and periodic nodal surfaces, *Appl. Therm. Eng.* 209 (2022). <https://doi.org/10.1016/j.applthermaleng.2022.118192>.
- [8] K. Yan, J. Wang, L. Li, H. Deng, Numerical investigation into thermo-hydraulic characteristics and mixing performance of triply periodic minimal surface-structured heat exchangers, *Appl. Therm. Eng.* 230 (2023). <https://doi.org/10.1016/j.applthermaleng.2023.120748>.
- [9] D. Liang, C. Shi, W. Li, W. Chen, M.K. Chyu, Design, flow characteristics and performance evaluation of bioinspired heat exchangers based on triply periodic minimal surfaces, *Int. J. Heat Mass Transf.* 201 (2023). <https://doi.org/10.1016/j.ijheatmasstransfer.2022.123620>.
- [10] W. Li, W. Li, Z. Yu, Heat transfer enhancement of water-cooled triply periodic minimal surface heat exchangers, *Appl. Therm. Eng.* 217 (2022). <https://doi.org/10.1016/j.applthermaleng.2022.119198>.
- [11] J. Wang, K. Chen, M. Zeng, T. Ma, Q. Wang, Z. Cheng, Investigation on flow and heat transfer in various channels based on triply periodic minimal surfaces (TPMS), *Energy Convers. Manag.* 283 (2023). <https://doi.org/10.1016/j.enconman.2023.116955>.
- [12] B.W. Reynolds, C.J. Fee, K.R. Morison, D.J. Holland, Characterisation of Heat Transfer within 3D Printed TPMS Heat Exchangers, *Int. J. Heat Mass Transf.* 212 (2023). <https://doi.org/10.1016/j.ijheatmasstransfer.2023.124264>.
- [13] H. Xu, W. Yu, Y. Zhang, S. Ma, Z. Wu, X. Liu, Flow and heat transfer performance of bionic heat transfer structures with hybrid triply periodic minimal surfaces, *Appl. Energy* 351 (2023). <https://doi.org/10.1016/j.apenergy.2023.121847>.
- [14] H. Peng, F. Gao, W. Hu, DESIGN, MODELING AND CHARACTERIZATION OF TRIPLY PERIODIC MINIMAL SURFACE HEAT EXCHANGERS WITH ADDITIVE MANUFACTURING, 2019 *Int. Solid Free. Fabr. Symp.* (2019). <https://doi.org/10.26153/tsw/17483>.
- [15] W. Li, G. Yu, Z. Yu, Bioinspired heat exchangers based on triply periodic minimal surfaces for supercritical CO₂ cycles, *Appl. Therm. Eng.* 179 (2020). <https://doi.org/10.1016/j.applthermaleng.2020.115686>.
- [16] T. Dixit, E. Al-Hajri, M.C. Paul, P. Nithiarasu, S. Kumar, High performance, microarchitected, compact heat exchanger enabled by 3D printing, *Appl. Therm. Eng.* 210 (2022). <https://doi.org/10.1016/j.applthermaleng.2022.118339>.
- [17] D. Liang, K. Yang, H. Gu, W. Chen, M.K. Chyu, The effect of unit size on the flow and heat transfer performance of the “Schwartz-D” heat exchanger, *Int. J. Heat Mass Transf.* 214 (2023). <https://doi.org/10.1016/j.ijheatmasstransfer.2023.124367>.

- [18] K. Yan, H. Deng, Y. Xiao, J. Wang, Y. Luo, Thermo-hydraulic performance evaluation through experiment and simulation of additive manufactured Gyroid-structured heat exchanger, *Appl. Therm. Eng.* 241 (2024). <https://doi.org/10.1016/j.applthermaleng.2024.122402>.
- [19] O. Al-Ketan, R.K. Abu Al-Rub, MSLattice: A free software for generating uniform and graded lattices based on triply periodic minimal surfaces, *Mater. Des. Process. Commun.* 3 (2021). <https://doi.org/10.1002/mdp2.205>.
- [20] S. Samson, P. Tran, P. Marzocca, Design and modelling of porous gyroid heatsinks: Influences of cell size, porosity and material variation, *Appl. Therm. Eng.* 235 (2023) 121296. <https://doi.org/10.1016/j.applthermaleng.2023.121296>.
- [21] J. McMurray, T. Besmann, J. Ard, B. Fitzpatrick, M. Piro, J. Jerden, M. Williamson, B. Collins, B. Betzler, A. Qualls, Multi-Physics Simulations for Molten Salt Reactor Evaluation: Chemistry Modeling and Database Development, 2018. <https://doi.org/10.2172/1492183>.
- [22] M.R. Campbell, M. Newmarker, N. Lewis, C.T. George, G. Cohen, Design of a Modular Latent Heat Storage System for Solar Thermal Power Plants, in: *American Society of Mechanical Engineers Digital Collection*, 2012: pp. 679–685. <https://doi.org/10.1115/ES2011-54426>.
- [23] V.N. Desyatnik, S.F. Katyshev, S.P. Raspopin, Yu.F. Chervinskii, Density, surface tension, and viscosity of uranium trichloride-sodium chloride melts, *Sov. At. Energy* 39 (1975) 649–651. <https://doi.org/10.1007/BF01121527>.
- [24] A. Dybbs, R.V. Edwards, A New Look at Porous Media Fluid Mechanics — Darcy to Turbulent, in: J. Bear, M.Y. Corapcioglu (Eds.), *Fundam. Transp. Phenom. Porous Media*, Springer Netherlands, Dordrecht, 1984: pp. 199–256. https://doi.org/10.1007/978-94-009-6175-3_4.
- [25] Z. Cheng, X. Li, R. Xu, P. Jiang, Investigations on porous media customized by triply periodic minimal surface: Heat transfer correlations and strength performance, *Int. Commun. Heat Mass Transf.* 129 (2021). <https://doi.org/10.1016/j.icheatmasstransfer.2021.105713>.
- [26] S. Mondal, R.W. Field, Theoretical analysis of the viscosity correction factor for heat transfer in pipe flow, *Chem. Eng. Sci.* 187 (2018) 27–32. <https://doi.org/10.1016/j.ces.2018.04.047>.
- [27] E.N. Sieder, G.E. Tate, Heat Transfer and Pressure Drop of Liquids in Tubes, *Ind. Eng. Chem.* 28 (1936) 1429–1435. <https://doi.org/10.1021/ie50324a027>.